Role of communication network topology in controlling microbial population in consortia

Xinying Ren Richard M. Murray

***Abstract*— Engineering microbial consortia is an important new frontier for synthetic biology given its efficiency in performing complex tasks and endurance to environmental uncertainty. Most synthetic circuits regulate populational behaviors via cell-to-cell communications, which are affected by spatially heterogenous environments. Therefore, it is important to understand the limits on controlling system dynamics that are determined by interconnections among cell agents and provide a control strategy for engineering consortia. Here, we build a network model for a fractional population control circuit in two-strain consortia, and characterize the cell-to-cell communication network by topological properties, such as symmetry, locality and connectivity. Using linear network control theory, we relate the network topology to system output's tracking performance. We analytically and numerically demonstrate that the minimum network control energy for accurate tracking depends on locality difference between two cell population's spatial distributions and how strongly the controller node contributes to communication strength. To realize a robust consortia, we can manipulate the communication network topology and construct strongly connected consortia by altering chemicals in environments. Our results ground the expected cell population dynamics in its spatially organized communication network, and inspire directions in cooperative control in microbial consortia.**

I. INTRODUCTION

Synthetic biology provides biotechnologies to engineer cells and organisms with pre-specified functions. Current synthetic gene circuits are mostly designed within single strain and the functions are operated at single-cell level [1]–[3]. However, collectives of cells can perform more complicated tasks and be more robust to environmental fluctuations than a single strain. Interest has recently emerged in designing synthetic circuits for collective behaviors in consortia, which include metabolites trading for mutualism in co-culture [4], programmed predation and rescue in prey-predator systems [5], and other competition or coordination in sender-receiver systems [6]. Multiple populations communicate with each other, divide labor and perform subtasks so that the overall control goal can be achieved in consortia. Therefore, engineering microbial consortia will enrich the potential of synthetic gene circuits in gene therapy, biofuel and other applications [7], [8].

Realizing proposed behaviors of multiple interacting strains on diverse temporal or spatial scales relies on two perspectives. First, synthetic gene circuits need to be engineered in each population to exhibit certain functions. Second, it is essential to engineer cell-to-cell communication to construct consortia. Bacteria have evolved communications by producing, exporting and sensing autoinducers that are mostly small and diffusible signaling molecules. This phenomenon is called quorum sensing, where the accumulation of autoinducers in environment provides a good measure of cell population density and can quantitatively affect a cell's gene expression or trigger a differentiation process [9]. Engineered communication with dedicated signal molecules are used to coordinate population level behaviors, such as cell suicide [10], pattern formation [11], and biofilm formation [12]. Existing work in ecology demonstrate that the cooperative behaviors in consortia rely on the spatial distribution of multiple cell agents and the structure of their communication [13]. Efforts in network science provide a good approach to define this spatial cell-to-cell communication as a network graph, to describe the consortia as an integrated system and to analyze population level performance and robustness by graph metrics [14]. Many forms of network characteristics can determine system behaviors of complex networks such as human brain [15], gene regulatory networks [16] and social networks [17], and specific features of network topology usually play a big role [18], [19]. As multiple cell populations are usually spatially organized and form heterogeneous consorta, understanding the relationship between cell-to-cell communication network topology and cooperative dynamics in consortia is particular useful for system-level controller design in synthetic biology. By linking the communication network topology to populational behaviors, one can optimize control objectives by rearranging the spatial distribution of cell agents, rewiring intercellular quorum sensing pathways, reweighting communication signaling strengths and turning on or off the synthetic circuits in certain cell agents via external chemical stimulations.

Recent research on engineering microbial consortia mainly focuses on intracellular circuit design [20], [21]. These papers assume that cell populations are well-mixed, because it is elusive how structured network properties enhance control potentials in spatial-organized consortia. Here, we propose a network control strategy of existing synthetic circuits and take different spatial distributions of cell agents and their communication structures into consideration. Although the principles derived here are based on a specific synthetic circuit that regulates cell population via toxin/antitoxin mechanism, they can be applied to a more general design framework, where the autoinducers in quorum sensing and their regulated products are included in a feedback controller at DNA, transcriptional and translational levels.

This paper is organized as follow. In Section II, we give an

X. Ren and R. M. Murray are with the Department of Control and Dynamical Systems, California Institute of Technology, Pasadena, CA. Email: xrren@caltech.edu.

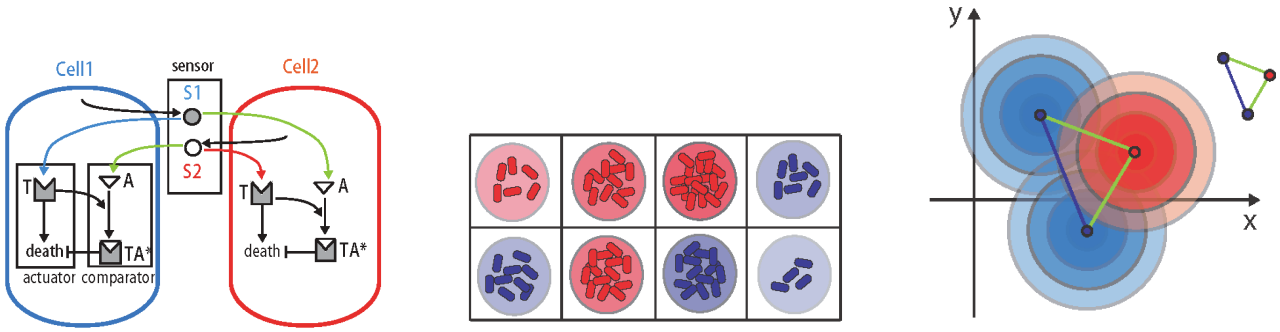

(a) (b) (c)

Fig. 1. Abstract biological design of fractional population control circuit and spatial settings. (a) describes toxin-antitoxin sequestration based fractional population control circuit. Two cell population communicate via two quorum sensing signals S_1, S_2. In $Cell_1$, S_1 activates toxin T and S_2 activates antitoxin A production to further regulate cell death and rescue processes through T and A sequestration. Similar reactions occur in $Cell_2$. (b) describes the spatial setting of microcolonies cultured on an ager plate. Two cell populations are grown in separate wells where quorum sensing signals can diffuse around and accumulate in environment to form a certain concentration distribution on 2D space. (c) describes the diffusion of AHL molecules and the color shades represent AHL concentration levels. Cell microcolonies are represented as point sources of AHLs and the concentration of AHLs decreases along distance to the source following the diffusion law. The colored lines between microcolonies represent inter-strain or intra-strain communications.

overview of the biological design of the synthetic circuit. It performs as a fractional population controller in *E.coli* [22], [23]. In Section III, we construct a reaction-diffusion model under spatial settings to describe the full dynamics of the system. In Section IV, we derive a reduced network model and define network topology properties such as symmetry, locality and connectivity. In Section V, we use linear network control theory to obtain a mathematical approximation of the closed-form solution for system steady state. Our results include a computational simulation and a mathematical proof relating the communication network topology properties to steady state cell populations. The results also include a graph representation of network topologies that are robust to perturbations, and potential ways of modifying the network topologies to steer system states in a predictable manner. We summarize the main findings of the paper discuss future work in Section VI.

II. BIOLOGICAL DESIGN

To engineer a stable co-culture of two cell strains $Cell_1$ and $Cell_2$ characterized by referenced fractional populations, we require a synthetic circuit that consists of a biological sensor, a population comparator/controller and a cell growth actuator. The sensors are achieved by identifying a small library of quorum sensing signaling molecules (acyl homoserine lactones, AHLs) and corresponding receptor-promotor pairs. Two cell strains produces orthogonal AHLs respectively and concentrations of AHLs are approximations for their population densities. Both AHLs can bind with constitutive promoters to activate expression of toxin ccdB and antitoxin ccdA [24]. The comparator/controller is constructed by sequestration of the AHL-induced toxin/antitoxin pair to compare two scaled up cell population densities. The toxin ccdB functions as the actuator to regulate cell growth by inhibiting cell proliferation. The synthetic circuit is shown in Fig. 1(a). The reference is set by the external IPTG level that induce AHL synthesis rate so that teh two cell populations achieve a controlled fraction in consortia. The circuit has good tracking accuracy of the reference and robust adaptation because it includes a sequestration-based controller that can be approximated as an integral feedback [25]–[27].

If cells are cultured in a well-mixed environment where we can assume cells of the same strain behave in an identical manner, the proposed intracellular synthetic circuit ensures that two AHLs are of approximately equal amounts everywhere at steady state. Thus, the population fraction is under good control. Alternatively, colonies can be cultured in a spatially heterogeneous pattern and AHL concentration forms a spatial distribution because of diffusion on agar plate. To regulate the relative ratio between cell population densities of two strains, one needs to introduce a network control input on consortia to compensate for effects caused by the spatial structure.

III. REACTION-DIFFUSION MODEL

We consider N microcolonies of strain $Cell_1$ and N microcolonies of strain $Cell_2$ cultured within $2N$ wells on an agar plate, as in Fig. 1(b). We assume that the microcolonies are shaped in circles centered at each well and grow within their boundaries. AHLs diffuse fast and freely in space as well as across the cell membrane and get degraded at a constant rate. Fig. 1(c) shows that AHL concentrations form certain distributions on 2D space. Dynamics of cells grown in the same well are assumed to be identical and are modeled as one agent, so the intracellular chemical kinetics can be reduced to a smaller equation set.

Our proposed reaction-diffusion model consists of $2N$ sets of ODEs of intracellular chemical dynamics and 2 sets of PDEs describing AHL diffusion and degradation in the environment. Species and reactions are shown in Table. I.

TABLE I

SPECIES AND BIOCHEMICAL REACTIONS

Species	Description
$C_i^{(1)}, C_j^{(2)}$	Cell population density of the ith, j^{th} microcolony of strain $Cell_1, Cell_2$
$T_i^{(1)}, T_j^{(2)}$	Intracellular toxin concentration of the ith, j^{th} microcolony of strain $Cell_1, Cell_2$
$A_i^{(1)}, A_j^{(2)}$	Intracellular antitoxin concentration of the ith, j^{th} microcolony of strain $Cell_1, Cell_2$
$S^{(1)}(\mathbf{r}), S^{(2)}(\mathbf{r})$	Concentration of AHL at position $\mathbf{r}$ produced by $Cell_1, Cell_2$
Reactions	**Description**
$C \xrightarrow{k_C logist(C)} 2C$	Cell growth and division
$C \xrightarrow{d_C T + \gamma} \varnothing$	Cell death by toxin effect and basal dilution
$\varnothing \xrightarrow{k_T hill(S)} T$	AHL activated production of toxin
$\varnothing \xrightarrow{k_A hill(S)} A$	AHL activated production of antitoxin
$T + A \underset{k^+}{\overset{k^-}{\rightleftharpoons}} TA^*$	Annihilating sequestration of toxin and antitoxin
$T \xrightarrow{d_T} \varnothing$	Degradation of toxin
$A \xrightarrow{d_A} \varnothing$	Degradation of antitoxin
$\varnothing \xrightarrow{k_S + k_{dif}\nabla} S$	Production and incoming diffusion flow of AHL
$S \xrightarrow{d_S + k_{dif}\nabla + \gamma} \varnothing$	Degradation, outgoing diffusion flow and dilution of AHL

$$
\begin{aligned}
\frac{\mathrm{d}C_i^{(1)}}{\mathrm{d}t} &= k_C\left(1-\frac{C_i^{(1)}}{C_{\max}}\right)C_i^{(1)} - d_C T_i^{(1)} C_i^{(1)} - \gamma C_i^{(1)} \\
\frac{\mathrm{d}T_i^{(1)}}{\mathrm{d}t} &= k_T \frac{\left(S^{(1)}\left(\mathbf{r}_i^{(1)}\right)\right)^2}{K_S + \left(S^{(1)}\left(\mathbf{r}_i^{(1)}\right)\right)^2} - k^+ T_i^{(1)} A_i^{(1)} - d_T T_i^{(1)} \\
\frac{\mathrm{d}A_i^{(1)}}{\mathrm{d}t} &= k_A \frac{\left(S^{(2)}\left(\mathbf{r}_i^{(1)}\right)\right)^2}{K_S + \left(S^{(2)}\left(\mathbf{r}_i^{(1)}\right)\right)^2} - k^+ T_i^{(1)} A_i^{(1)} - d_A A_i^{(1)} \\
\frac{\partial S^{(1)}(\mathbf{r},t)}{\partial t} &= \sum_{p=1}^{N} \frac{k_S}{r_y} C_p^{(1)} \mathbb{1}_{\{\mathbf{r}=\mathbf{r}_p^{(1)}\}}(\mathbf{r}) + k_{dif}\nabla^2 S^{(1)}(\mathbf{r},t) \\
&\quad - (d_S+\gamma) S^{(1)}(\mathbf{r},t) \\
0 \le |\mathbf{r}| \le L, S^{(1)}(\mathbf{r},0) &= 0, S^{(1)}\left(L\frac{\mathbf{r}}{|\mathbf{r}|},t\right) = 0 \\
\frac{\partial S^{(2)}(\mathbf{r},t)}{\partial t} &= \sum_{q=1}^{N} k_S C_q^{(2)} \mathbb{1}_{\{\mathbf{r}=\mathbf{r}_q^{(2)}\}}(\mathbf{r}) + k_{dif}\nabla^2 S^{(2)}(\mathbf{r},t) \\
&\quad - (d_S+\gamma) S^{(2)}(\mathbf{r},t) \\
0 \le |\mathbf{r}| \le L, S^{(2)}(\mathbf{r},0) &= 0, S^{(2)}\left(L\frac{\mathbf{r}}{|\mathbf{r}|},t\right) = 0
\end{aligned} \tag{1}
$$

Eq(1) describes the dynamics of cell growth and toxin-antitoxin kinetics in microcolonies of $Cell_1$ indexed by $i = 1,2,\ldots,N$, and reaction-diffusion equations and boundary constraints for two AHLs. Similar dynamics of $Cell_2$ and intracellur chemical kinetics in microcolonies indexed by $j = 1,2,\ldots,N$ exist. They are not presented in eq(1).

For the well-mixed case shown in Fig. 2(a), we set the distance unit between two adjacent wells to be value 0 and run simulations on the full model given different references. Fig. 2(b) shows that the output dynamics converge to reference with nearly zero error.

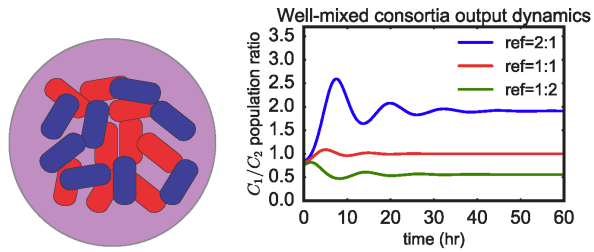

(a) (b)

Fig. 2. Well-mixed consortia with fractional population control circuit. (a) is a sketch for physically well-mixed consortia. Two cell populations are represented in blue for $Cell_1$ and red for $Cell_2$, and the purple background shows the well-mixed environment of two AHLs. (b) describes the output dynamics with different references set by external IPTG inducer levels. The output converges to reference with negligible error at steady state.

For spatially distributed consortia, we can reduce the full model into a simplified one that captures dynamics of intracellular chemicals and cell-to-cell communications. We first reduce the PDEs using quasi-steady state assumptions, and then reduce the ODEs by linearization. AHL molecules normally diffuse fast on an agar plate [28] so the timescale of AHL dynamics is smaller than trascriptional and translational chemical dynamics in cells. We assume the AHL concentration distribution on 2D space reaches a quasi-steady state. Since AHL molecules only affect cell populations when they get absorbed by cells and react with intracellular chemicals, we only solve for such quasi-steady states of the AHL concentration at each $Cell_1$ microcolony according to PDEs in eq(

$$
\begin{aligned}
S^{(1)}\left(\mathbf{r}_i^{(1)}\right) &= \frac{K_{dif}}{r_y}\sum_{p=1}^{N} f\left(\mathbf{r}_p^{(1)} - \mathbf{r}_i^{(1)}\right) C_p^{(1)}, \\
S^{(2)}\left(\mathbf{r}_i^{(1)}\right) &= K_{dif}\sum_{q=1}^{N} f\left(\mathbf{r}_q^{(2)} - \mathbf{r}_i^{(1)}\right) C_q^{(2)}, \\
K_{dif} = \frac{k_S}{2\sqrt{k_{dif}(d_S+\gamma)}}&, f(\mathbf{r}) = \exp\left(-\sqrt{\frac{d_S+\gamma}{k_{dif}}}|\mathbf{r}|\right).
\end{aligned} \tag{2}
$$

The cell population is regulated by toxin concentration. Since the toxin-antitoxin pair performs strong sequestration, there is a timescale separation of toxin dynamics from cell growth. By peroforming quasi-steady state approximation and linearization on ODEs in eq(1), we can further reduce the model that only contains cell population densities as variables, in forms of

$$
\begin{aligned}
\frac{\mathrm{d}C_i^{(1)}}{\mathrm{d}t} &= \frac{k_T d_C}{d_T}\left(-\frac{1}{r_y}S^{(1)}\left(\mathbf{r}_i^{(1)}\right) + S^{(2)}\left(\mathbf{r}_i^{(1)}\right)\right), \\
\frac{\mathrm{d}C_j^{(2)}}{\mathrm{d}t} &= \frac{k_T d_C}{d_T}\left(\frac{1}{r_y}S^{(1)}\left(\mathbf{r}_j^{(2)}\right) - S^{(2)}\left(\mathbf{r}_j^{(2)}\right)\right).
\end{aligned} \tag{3}
$$

We plug eq(2) into eq(3), and obtain a reduced model as

$$
\begin{aligned}
\frac{\mathrm{d}C_i^{(1)}}{\mathrm{d}t} &= K_C\left(-\frac{1}{r_y}\sum_{p=1}^{N} f\left(\mathbf{r}_p^{(1)}-\mathbf{r}_i^{(1)}\right)C_p^{(1)}+\sum_{q=1}^{N} f\left(\mathbf{r_q}^{(2)}-\mathbf{r}_i^{(1)}\right)C_q^{(2)}\right),\\
\frac{\mathrm{d}C_j^{(2)}}{\mathrm{d}t} &= K_C\left(+\frac{1}{r_y}\sum_{p=1}^{N} f\left(\mathbf{r}_p^{(1)}-\mathbf{r}_j^{(2)}\right)C_p^{(1)}-\sum_{q=1}^{N} f\left(\mathbf{r}_q^{(2)}-\mathbf{r}_j^{(2)}\right)C_q^{(2)}\right),
\end{aligned}
\tag{4}
$$

where $K_C = \frac{K_{dif}k_T d_C}{d_T}$.

IV. NETWORK MODEL AND TOPOLOGY PROPERTIES

We consider a network model for spatially distributed consortia and the network can be represented by a fully connected graph $G = \{V, E\}$ where $V = \{1, 2, \cdots, 2N\}$ and $E \in V \times V$ are the sets of vertices and edges. The vertices are microcolonies and edges are cell-to-cell communication pathways via quorum sensing. We define the weighted adjacent matrix $D = [d_{ij}] \in \mathbb{R}^{2N\times 2N}$. The element of d_{ij} represents the communication strength associated with the corresponding edge in E.

The network graph can be partitioned into four subnetwork graphs: G_{11}, G_{22} containing only microcolonies of one cell population as nodes and communication edges among these nodes, and G_{12}, G_{21} containing cell microcolonies of both population as nodes but only communication edges from one cell population to another. Similarly, the matrix D can be partitioned into four blocks and they are referred as intra-strain communication strength matrix $-D_{11}$, $-D_{22}$, and inter-strain communication strength matrix D_{12}, D_{21}. We associate a set of real values of cell population densities of each microcolon as system states, denoted as $C_i^{(1)}, C_j^{(2)}, i, j = 1, 2, \ldots, N$, and combine these states into a big network state vector $X = [X^{(1)}, X^{(2)}]^T = [C_1^{(1)} \cdots C_N^{(1)} C_1^{(2)} \cdots C_N^{(2)}]^T \in \mathbb{R}^{2N}$.

We identify the element d_{ij} of matrix D as a function of geometric distance between nodes with lumped biophysical parameters, and derive the network state dynamics according to eq(4). Let the output be the relative ratio between two cell population densities. We use l_2 norm for all following discussions.

$$
\begin{aligned}
\frac{\mathrm{d}}{\mathrm{d}t}\begin{bmatrix} X^{(1)} \\ X^{(2)} \end{bmatrix} &= \begin{bmatrix} -\frac{1}{r_y}D_{11} & D_{12} \\ \frac{1}{r_y}D_{21} & -D_{22} \end{bmatrix}\begin{bmatrix} X^{(1)} \\ X^{(2)} \end{bmatrix} + \begin{bmatrix} -D_{11} \\ D_{21} \end{bmatrix}\mathbf{u}\\
y &= \frac{\left\|X^{(1)}\right\|}{\left\|X^{(2)}\right\|}
\end{aligned}
\tag{5}
$$

Our overall control goal is to set the output to track an external reference r_y, set by IPTG inducer level on AHL_1 synthases. We add a network control input $\mathbf{u} \in \mathbb{R}^N$ into the system, and it is implemented as an extra production of AHL_1 in each $Cell_1$ well. Therefore, the coefficient matrix of $\mathbf{u}$ depends on matrix D in such form in eq(5). When two cell populations are grown on a plate, the spatially structured communication network may require a control input $\mathbf{u}$ to steer the system to the steady state that satisfies the reference r_y. We define the energy of $\mathbf{u}$ as $EN(\mathbf{u}) = \sum_{i=1}^{N} u_i^2$, where u_i are elements of $\mathbf{u}$, $i = 1, 2, \cdots, N$.

To characterize the topology of the communication network and seek a tractable link from topology to system dynamics and control energy, we define topology properties such as symmetry, locality and connectivity in the context of quorum sensing in microbial consortia.

Consider a network $G = \cup G_{ij}, i, j = 1, 2$ with adjacent matrix $D = \begin{bmatrix} -D_{11} & D_{12} \\ D_{21} & -D_{22} \end{bmatrix}$.

Definition 1. *If $D_{11} = D_{22}$, $D_{12} = D_{21}$, then G is a symmetrical network.*

Remark. Assuming two AHLs diffuse and get degraded at the same rate, the geometric symmetry of spatially distributed consortia is equivalent to network topology symmetry.

Definition 2. *The locality of a subnetwork G_{ii} is defined as $\|D_{ii}\|, i = 1, 2$.*

Remark. Locality measures the intra-strain communication strength. If microcolonies aggregate closer in geometry, they form a more localized community.

Definition 3. *The connectivity of a subnetwork G_{ij} is defined as $\left\|D_{ij}\right\|, i, j = 1, 2, i \neq j$. Connectivity of a network G is defined as $\left\|D_{ij}\right\| + \left\|D_{ji}\right\|, i, j = 1, 2, i \neq j$.*

Remark. Connectivity represents the inter-strain communication strength. If two cell populations are more mixed than isolated, the network is strongly connected with large connectivity. Otherwise, the network is weakly connected.

Remark. Within a network G, we can further measure the contribution of each node to network locality and connectivity. For example, the ith $Cell_1$ microcolony's contribution to network locality is computed as the norm of the ith column vector of D_{11} and contribution to connectivity is computed as the norm of the ith column vector of D_{21}.

V. RELATIONSHIP BETWEEN TOPOLOGY AND SYSTEM BEHAVIORS

The results from previous work on this synthetic fractional population controller shows thqt the output y of the system converges to a constant reference r_y with negligible error under well-mixed assumptions. The output's accurate tracking performance may not maintain under spatial settings.

$$
\begin{aligned}
\underset{G}{\text{minimize}} \quad & EN(\mathbf{u})\\
\text{subject to} \quad & G \in \{G\},\\
& y_\infty \to r_y, t \to \infty\\
& \mathbf{u} = [1, \cdots, 1]^T u.
\end{aligned}
\tag{6}
$$

To gain an understanding of constraints on spatially organized network topology for good output tracking, we first set the network control input $\mathbf{u}$ to be zero and solve for output dynamics of all potential network topologies. Then we look for certain topologies that need small control efforts by solving the optimization problem in eq(6). The network topology is characterized by symmetry, locality and connectivity, and we can derive an approximated function

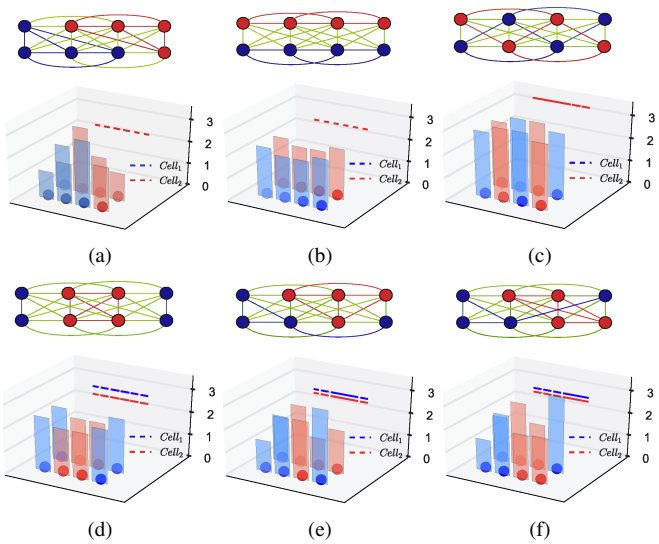

Fig. 3. System steady states for spatially cultured consortia with symmetrical or asymmetrical communication networks. (a)-(c) describe consortia structures with different symmetrical network topologies, denoted as sym1, sym2 and sym3. The upper plots are network graph representations. Blue and red nodes are microcoloinies of two cell populations; blue and red edges are intra-strain communication pathways; green edges are inter-strain communication pathways. The lower plots show cell population density at steady state. The bars are population densities of each microcolony and the dashed lines (blue and red) on $x-z$ plane are total $Cell_1$ population and total $Cell_2$ population. The dashed lines overlap, indicating that the relative population ratio between two strains is value 1, so $y_\infty = r_y$. These examples demonstrate symmetrical network topologies ensure good control performance of output via intercellular synthetic circuit in terms of tracking accuracy without extra network control. (d)-(f) describe consortia structures with different asymmetrical network topologies, denoted as asym1, asym2 and asym3. The dashed lines are not at same level, indicating that the output doesn't perform good tracking and the system needs an network control input to achieve referenced cell population fraction.

showing how these properties contribute to the minimum required network control energy.

$$\begin{aligned} \underset{i}{\text{minimize}} \quad & EN(\mathbf{u}) \\ \text{subject to} \quad & G = \{V,E\} \text{ with } D = \begin{bmatrix} -D_{11} & D_{12} \\ D_{21} & -D_{22} \end{bmatrix} \\ & y_\infty \to r_y, t \to \infty \\ & \mathbf{u} = [0,\cdots,0,1,0,\cdots,0]^T u. \end{aligned} \tag{7}$$

Given a certain network topology, we further identify energetically favorable controller nodes and give a selection principle of the most or least favorable node. The question can be formulated as an optimization problem in eq(7).

We present propositions and give math proof sketch and simulation results for demonstration.

A. Network symmetry determines system tracking accuracy

Proposition 1. *If network G is symmetrical, then it requires no network control input energy to achieve accurate tracking performance in output y at steady state.*

Proof Let $\mathbf{u} = \mathbf{0}$, the system dynamics is reduced to

$$\frac{\mathrm{d}}{\mathrm{d}t}\begin{bmatrix} X^{(1)} \\ X^{(2)} \end{bmatrix} = \begin{bmatrix} -\frac{1}{r_y}D_{11} & D_{12} \\ \frac{1}{r_y}D_{21} & -D_{22} \end{bmatrix}\begin{bmatrix} X^{(1)} \\ X^{(2)} \end{bmatrix}. \tag{8}$$

Since G is symmetrical, we have $D_{11} = D_{22}$, $D_{12} = D_{21}$. By subtraction of $X^{(1)}$ and $X^{(2)}$ dynamics in eq(5), we can obtain the dynamics of $\Delta X = X^{(1)} - X^{(2)}$ as

$$\frac{\mathrm{d}(\Delta X)}{\mathrm{d}t} = (D_{11}+D_{12})\left(X^{(2)} - \frac{1}{r_y}X^{(1)}\right). \tag{9}$$

If there is a steady state, we can solve for the solution.

$$y_\infty = \frac{\left\|X_\infty^{(1)}\right\|}{\left\|X_\infty^{(2)}\right\|} = r_y \tag{10}$$

■

Simulation

We run simulations on the full reaction-diffusion model in eq(1). There are $N = 4$ microcolonies of both cell population $Cell_1$, $Cell_2$, spatially distributed in $2N$ wells. For simplicity, we set the IPTG inducer level that leads to reference $r_y = 1$. We set control input $\mathbf{u} = \mathbf{0}$. We present three different network topologies that are symmetrical, labeled as sym1, sym2 and sym3 in Fig. 3(a)-3(c). The figures illustrate network topologies in graph representations and show the system state values (cell population densities) on 2D space at steady state. Fig. 4(a) shows the output's dynamics. Computational results match with the proposition that output converges to value 1 without extra network control input.

B. Locality identifies topology that requires minimum control energy

Proposition 2. *If network G is asymmetrical, then the minimum network control input energy required for accurate tracking depends on the locality difference between subnetworks G_{11} and G_{22}.*

$$\begin{aligned} \arg\min_G EN(\mathbf{u}) &= \arg\min_G |\|D_{22}\| - \|D_{11}\|| \\ \arg\max_G EN(\mathbf{u}) &= \arg\max_G |\|D_{22}\| - \|D_{11}\|| \end{aligned} \tag{11}$$

Proof Let $\mathbf{u} = [1,\cdots,1]^T u$. By subtraction of $X^{(1)}$ and $X^{(2)}$ dynamics in eq(5), we can obtain

$$\frac{\mathrm{d}(\Delta X)}{\mathrm{d}t} = -(D_{11}+D_{21})\left(\frac{1}{r_y}X^{(1)} + u\right) + (D_{12}+D_{22})X^{(2)}. \tag{12}$$

If there is a steady state, we can solve for the solution.

$$X_\infty^{(1)} = r_y(D_{11}+D_{21})^{-1}(D_{12}+D_{22})X_\infty^{(2)} - r_y u \tag{13}$$

To achieve referenced output, we let $y_\infty = r_y$ and solve for the minimum required control input energy by giving inequalities.

$$EN(\mathbf{u}) = N\|u\| \geq \frac{N\left\|X_\infty^{(2)}\right\|}{\|D_{11}\|+\|D_{21}\|}\,|\|D_{22}\| - \|D_{11}\|| \tag{14}$$

For all network topologies in fixed $2N$ wells, $\|D_{11}\|+\|D_{21}\|$ is constant and we can minimized the control energy by minimizing network locality difference. ■

Simulation Similarly, we set the reference $r_y = 1$. We

present three different network topologies that are asymmetrical, labeled as asym1, asym2 and asym3 in Fig. 3(d)-3(f). For all these topologies, $Cell_2$ are more locally distributed than $Cell_1$, which satisfy $\|D_{22}\| - \|D_{11}\| > 0$. Fig. 3(d)-3(f) demonstrate the system state values (cell population densities) on 2D space at steady state without network control input $\mathbf{u}$. They show $Cell_2$ population occupies a lower fraction than $Cell_1$, in other words, $y_\infty > r_y$. We then run simulations with network control input added to the systems and compare the output dynamics in Fig. 4(b). All three systems perform good tracking of the reference with different levels of control energy. We analyze all potential topologies for $N = 4$ spatial settings and plot the relationship between locality difference and steady state output without control input $\mathbf{u}$ in Fig. 4(c), and the relationship between locality difference and minimum required control energy in Fig. 4(d). We altered the absolute distance unit values between adjacent wells and the relationships maintain. The computational results verify the theoretical predictions. By analyzing the communication network topology, we can predict output steady state error and get knowledge on lower/upper bounds of required control energy to decrease error.

C. Locality and connectivity contribution identifies energetically favorable controller node

Proposition 3. *Given a network G, the selection of the most energetically favorable node depends on the node's contribution to locality and connectivity.*

$$\arg\min_i EN(\mathbf{u}) = \arg\max_i \left\| (D_{11} + D_{21}) \left[0, \cdots, 0, 1_{i-th}, 0, \cdots, 0\right]^T \right\| \tag{15}$$

Proof Let $\mathbf{u} = [0, \cdots, 0, 1_{i-th}, 0, \cdots, 0]^T u$. Let $v_i^{(11)}$ and $v_i^{(21)}$ denote the ith column of D_{11} and D_{21} as

$$\begin{aligned} v_i^{(11)} &= D_{11} \left[0, \cdots, 0, 1_{i-th}, 0, \cdots, 0\right]^T, \\ v_i^{(11)} &= D_{21} \left[0, \cdots, 0, 1_{i-th}, 0, \cdots, 0\right]^T. \end{aligned} \tag{16}$$

By subtraction of $X^{(1)}$ and $X^{(2)}$ dynamics in eq(5), we can obtain the dynamics of $\Delta X = X^{(1)} - X^{(2)}$ as

$$\begin{aligned} \frac{\mathrm{d}(\Delta X)}{\mathrm{d}t} &= -(D_{11} + D_{21}) \frac{1}{r_y} X^{(1)} + (D_{12} + D_{22}) X^{(2)} \\ &\quad - \left(v_i^{(11)} + v_i^{(21)}\right) u \end{aligned} \tag{17}$$

If there is a steady state, we can solve for the solution as

$$\begin{aligned} X_\infty^{(1)} &= r_y (D_{11} + D_{21})^{-1} (D_{12} + D_{22}) X_\infty^{(2)} \\ &\quad - (D_{11} + D_{21})^{-1} r_y \left(v_i^{(11)} + v_i^{(21)}\right) u. \end{aligned} \tag{18}$$

To achieve the referenced output, we let $y_\infty = r_y$ and solve for the minimum required control input energy as

$$EN(\mathbf{u}) = \|u\| \geq \left\| X_\infty^{(2)} \right\| \left| \|D_{22}\| - \|D_{11}\| \right| \frac{1}{\left\| v_i^{(11)} + v_i^{(21)} \right\|}. \tag{19}$$

Given a network topology, D is fixed and we can minimize the control energy by picking one favorable node that contribute most to locality and connectivity. ■

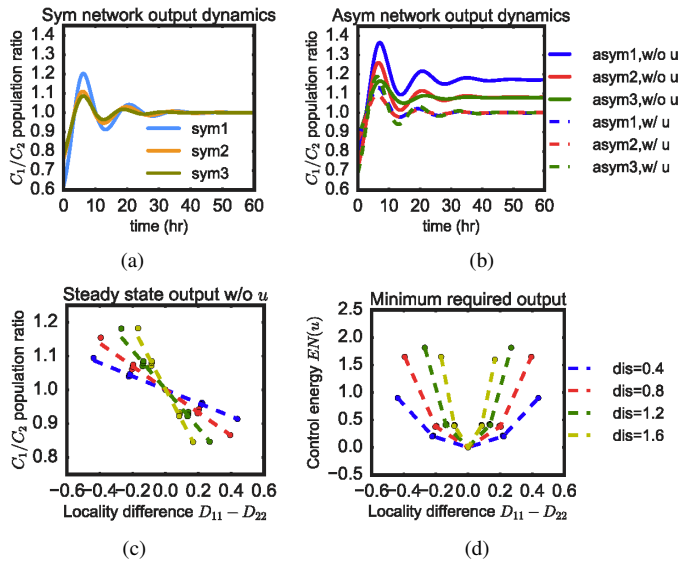

Fig. 4. System state and output dynamics w/ and w/o network control input. (a) describes output dynamics of three different symmetrical network topologies (sym1-3) without network control input u. Outputs of all symmetrical networks achieve reference at value 1. (b) describes output dynamics of three different asymmetrical network topologies (asym1-3). Solid lines represent outputs with no network control input u and there are significant steady state errors. Dashed lines represent outputs with minimum network control input u and all of them converge to the constant reference $r_y = 1$. (c) describes the relationship between steady state output and the difference between communication network localities of two cell populations. The dots are simulated data from all potential topologies of consortia cultured in $2N = 2 \times 4$ wells, and the dashed lines are fitted linear functions. Different colors represent results for different physical distance unit values between two adjacent wells. The plot shows that more localized cell population tends to occupy a lower population fraction. When $\|D_{11}\| \leq \|D_{22}\|$, we have $y_\infty r_y$ Networks that have the large locality difference achieve the big steady state error to in output without network control input. (d) describes the relationship between minimum required network control energy and the difference between communication network localities of two cell populations. The plot shows networks that have large locality difference require more control effort to track reference.

Simulation

We demonstrate the proposition by adding a constant network control input onto each node of a fixed network topology, and measure the control energy required for steering the system output to track the reference. Fig. 5 shows an example of asym1 network topology. Our results show that the maximizer and minimizer of function $\left\| (D_{11} + D_{21}) \left[0, \cdots, 0, 1_{i-th}, 0, \cdots, 0\right]^T \right\|$ are exactly the most and least energetically favorable nodes. The data show $\frac{EN(\mathbf{u})_{max}}{EN(\mathbf{u})_{min}} \approx 1.2$, so the worst selection of control nodes can result in 20% more of energy burden. The simulations are consistent with theory and provide insight to identify energetically favorable nodes to a linear control input given a fixed topology.

D. Connectivity improves network robustness

In microbial consortia, fluctuations of chemicals in environment can cause uncertainty and noises in cell growth. To investigate the robustness of our synthetic circuit and communication network, we introduce a metabolic burden

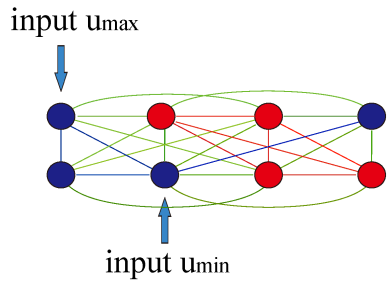

Fig. 5. Illustration for picking energetically favorable nodes for asymmetrical networks. The most energetically favorable node is the one in the network center, which contributes most to network's locality and connectivity. It has a more significant effect on system dynamics because it is strongly connected with other nodes.

change as a disturbance to cell growth, and assess system output's adaptation as a measure of robustness. For all potential network topologies, we decrease the growth rate of $Cell_1$ populations after the system achieves some steady states, and measure the output recovery error when the systems achieves steady states again. Fig. 6(a) shows that topologies of large connectivity are more adaptive to perturbations. Fig. 6(b) shows that the most robust network topology is sym3 where all $Cell_1$ and $Cell_2$ microcolonies are strongly connected, and the least robust network topology describes consortia that contain two rather isolated populations.

From an ecological perspective, our proposed population regulation circuit performs a similar mutualistic symbiosis. Research has shown that mixed consortia are more robust to environmental perturbations and more resistant to invaders [13]. Our model captures such property by relating communication network connectivity to robustness. In network graph representation, it is clear to see strongly connected topologies correspond to mixed consortia and weakly connected topologies correspond to isolated consortia.

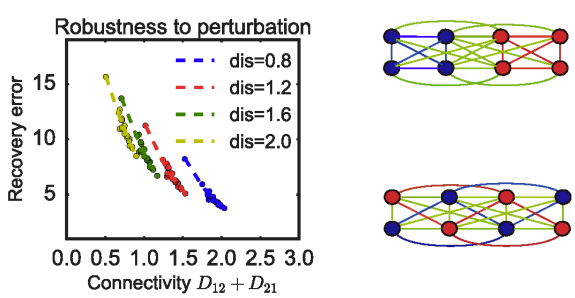

(a) (b)

Fig. 6. Robustness of networks under perturbations. (a) describes the relationship between network connectivity and output recovery error after $Cell_1$ growth rate is perturbed to be 20% slower. The dots are simulated data from all potential topologies of consortia cultured in $2N = 24$ wells, and the dashed lines are fitted linear functions. Different colors represents for different physical distance unit values between two adjacent wells. The plot shows that strongly connected networks are more robust than weakly connected networks with smaller output recovery error. Strongly connected networks have better adaptation to fluctuations in environments. (b) shows two network topologies that have the smallest(upper) and largest(lower) connectivity. Their corresponding systems are the least and most robust one over all potential networks.

E. Network topology manipulation to facilitate control

Here, we have represented four propositions showing the relationship between communication network topology and system dynamics. Proposition 2 shows that networks of small locality differences between two cell populations require less control energy. Symmetrical networks are a special case with zero locality difference and therefore ensure accurate reference tracking with zero network control input, as stated in Proposition 1. To better facilitate control with minimum effort, we can consider network modifications that decrease the locality difference by removing or adding nodes, reweighting and rewiring edges. Such methods can be implemented in microbial consortia by adding antibiotics, constraining nutrients in environments and using quorum sensing signals that diffuse at different rates for short/long range communication. These manipulations can be optimized according to specific forms of control input, for example unified constant input at all microcolonies or at one controller node. Proposition 3 helps to identify which single microcolony to target as a controller node given a fixed network. Meanwhile, the robustness of the system needs to be considered when doing modifications for improvement.

VI. DISCUSSION

In this paper, we propose a network control strategy to achieve population regulation for spatially distributed microbial consortia. Given a intracellular synthetic circuit, we focus on a physically meaningful understanding of how cell-to-cell communication network topology governs control potential. We build a network model based on reaction-diffusion equations, map system behaviors to topology properties and formulate the network control question as optimization problems. The propositions inform links from topology to dynamics analytically and numerically, and provide network level design guidance for better performance with less control efforts in synthetic biology problems.

We note that our work is based on a specific synthetic circuit, but the theory and analysis can be adopted to a more generalized problem in synthetic biology. For any functional intracellular circuit that requires cell-to-cell communication, our approach is useful for finding out constraints on spatial-temporal dynamics. In ecology, it is interesting to apply network control theory to understand and engineer multiple symbiotic relationships. It is important to discuss about such theoretical limitations on population level synthetic system design, such as biofilm formation. For future work, we would like to gain more intuition about the role of topology in complex networks by applying our results to other systems in microbial consortia. A challenge could be higher-order approximation for more complicated biochemical reactions to reduce the full model into a network model. More metrics on system dynamics are also worth exploring besides steady state evaluation.

VII. ACKNOWLEDGMENTS

The authors would like to thank Fangzhou Xiao and Leo Green for their insightful discussion. The authors X. R is

partially supported by the Air Force Office of Scientific Research, grant number FA9550-14-1-0060. The project depicted is also sponsored by the Defense Advanced Research Projects Agency (Agreement HR0011-17-2-0008). The content of the information does not necessarily reflect the position or the policy of the Government, and no official endorsement should be inferred.

REFERENCES

[1] J. Stricker, S. Cookson, M. R. Bennett, W. H. Mather, L. S. Tsimring, and J. Hasty, "A fast, robust and tunable synthetic gene oscillator," *Nature*, vol. 456, no. 7221, pp. 516–519, 2008.

[2] M. B. Elowitz and S. Leibler, "A synthetic oscillatory network of transcriptional regulators," *Nature*, vol. 403, no. 6767, pp. 335–338, 2000.

[3] T. S. Gardner, C. R. Cantor, and J. J. Collins, "Construction of a genetic toggle switch in escherichia coli," *Nature*, vol. 403, no. 6767, p. 339–342, 2000.

[4] L. Keller and M. G. Surette, "Communication in bacteria: an ecological and evolutionary perspective," *Nature Reviews Microbiology*, vol. 4, no. 4, p. 249, 2006.

[5] F. K. Balagaddé, H. Song, J. Ozaki, C. H. Collins, M. Barnet, F. H. Arnold, S. R. Quake, and L. You, "A synthetic escherichia coli predator–prey ecosystem," *Molecular Systems Biology*, vol. 4, no. 1, 2008.

[6] W. Weber, M. Daoud-El Baba, and M. Fussenegger, "Synthetic ecosystems based on airborne inter-and intrakingdom communication," *Proceedings of the National Academy of Sciences*, vol. 104, no. 25, pp. 10 435–10 440, 2007.

[7] D.-K. Ro, E. M. Paradise, M. Ouellet, K. J. Fisher, K. L. Newman, J. M. Ndungu, K. A. Ho, R. A. Eachus, T. S. Ham, J. Kirby, M. C. Y. Chang, S. T. Withers, Y. Shiba, R. Sarpong, and J. D. Keasling, "Production of the antimalarial drug precursor artemisinic acid in engineered yeast," *Nature*, vol. 440, no. 7086, pp. 940–943, 2006.

[8] J. J. Minty, M. E. Singer, S. A. Scholz, C.-H. Bae, J.-H. Ahn, C. E. Foster, J. C. Liao, and X. N. Lin, "Design and characterization of synthetic fungal-bacterial consortia for direct production of isobutanol from cellulosic biomass," *Proceedings of the National Academy of Sciences*, vol. 110, no. 36, pp. 14 592–14 597, 2013.

[9] W. C. Fuqua, S. C. Winans, and E. P. Greenberg, "Quorum sensing in bacteria: the luxr-luxi family of cell density-responsive transcriptional regulators." *Journal of bacteriology*, vol. 176, no. 2, p. 269, 1994.

[10] L. You, R. S. Cox, R. Weiss, and F. H. Arnold, "Programmed population control by cell–cell communication and regulated killing," *Nature*, vol. 428, no. 6985, pp. 868–871, 2004.

[11] S. Basu, Y. Gerchman, C. H. Collins, F. H. Arnold, and R. Weiss, "A synthetic multicellular system for programmed pattern formation," *Nature*, vol. 434, no. 7037, pp. 1130–1134, 2005.

[12] K. Brenner, D. K. Karig, R. Weiss, and F. H. Arnold, "Engineered bidirectional communication mediates a consensus in a microbial biofilm consortium," *Proceedings of the National Academy of Sciences*, vol. 104, no. 44, pp. 17 300–17 304, 2007.

[13] A. E. Escalante, M. Rebolleda-Gómez, M. Benítez, and M. Travisano, "Ecological perspectives on synthetic biology: insights from microbial population biology," *Frontiers in microbiology*, vol. 6, p. 143, 2015.

[14] M. Newman, *Networks: an introduction*. Oxford university press, 2010.

[15] D. S. Bassett and O. Sporns, "Network neuroscience," *Nature neuroscience*, vol. 20, no. 3, p. 353, 2017.

[16] R. Milo, S. Shen-Orr, S. Itzkovitz, N. Kashtan, D. Chklovskii, and U. Alon, "Network motifs: simple building blocks of complex networks," *Science*, vol. 298, no. 5594, pp. 824–827, 2002.

[17] J. Scott, *Social network analysis*. Sage, 2017.

[18] D. J. Watts and S. H. Strogatz, "Collective dynamics of 'small-world'networks," *nature*, vol. 393, no. 6684, p. 440, 1998.

[19] H. A. Simon, "The architecture of complexity," in *Facets of systems science*. Springer, 1991, pp. 457–476.

[20] Y. Chen, J. K. Kim, A. J. Hirning, K. Josić, and M. R. Bennett, "Emergent genetic oscillations in a synthetic microbial consortium," *Science*, vol. 349, no. 6251, pp. 986–989, 2015.

[21] G. Fiore, A. Matyjaszkiewicz, F. Annunziata, C. Grierson, N. J. Savery, L. Marucci, and M. di Bernardo, "Design of a multicellular feedback control strategy in a synthetic bacterial consortium," in *Decision and Control (CDC), 2016 IEEE 55th Conference on*. IEEE, 2016, pp. 3338–3343.

[22] X. Ren, A.-A. Baetica, A. Swaminathan, and R. M. Murray, "Population regulation in microbial consortia using dual feedback control," 2017.

[23] R. D. McCardell, S. Huang, L. N. Green, and R. M. Murray, "Control of bacterial population density with population feedback and molecular sequestration," *bioRxiv*, p. 225045, 2017.

[24] E. M. Bahassi, M. H. O'Dea, N. Allali, J. Messens, M. Gellert, and M. Couturier, "Interactions of ccdb with dna gyrase inactivation of gyra, poisoning of the gyrase-dna complex, and the antidote action of ccda," *Journal of Biological Chemistry*, vol. 274, no. 16, pp. 10 936–10 944, 1999.

[25] K. J. Aström and R. M. Murray, *Feedback systems: an introduction for scientists and engineers*. Princeton university press, 2010.

[26] C. Briat, A. Gupta, and M. Khammash, "Antithetic integral feedback ensures robust perfect adaptation in noisy biomolecular networks," *Cell systems*, vol. 2, no. 1, pp. 15–26, 2016.

[27] N. Olsman, A.-A. Baetica, F. Xiao, Y. P. Leong, J. Doyle, and R. Murray, "Hard limits and performance tradeoffs in a class of sequestration feedback systems," *bioRxiv*, 2017. [Online]. Available: https://www.biorxiv.org/content/early/2017/11/20/222042

[28] A. W. Decho, R. L. Frey, and J. L. Ferry, "Chemical challenges to bacterial ahl signaling in the environment," *Chemical Reviews*, vol. 111, no. 1, pp. 86–99, 2011, pMID: 21142012. [Online]. Available: https://doi.org/10.1021/cr100311q